

AN ATLAS OF STATIONARY BOW SHOCK ARCS IN THE ORION NEBULA

WILLIAM J. HENNEY, LUIS A. GUTIÉRREZ-SOTO, JORGE A. TARANGO-YONG

Centro de Radioastronomía y Astrofísica, Universidad Nacional Autónoma de México, Apartado Postal 3-72, 58090 Morelia, Michoacán, Mexico;
w.henney@crya.unam.mx, l.gutierrez@crya.unam.mx, j.tarango@crya.unam.mx

Draft version January 28, 2015

Abstract

We present a complete catalog of all the stationary emission line arcs (LL objects and proplyd bowshocks) found in archival HST imaging of the Orion Nebula. The total number of objects detected is 73, of which 20 have not previously been reported in the literature. We classify the shapes of emission line arcs by fitting conic sections to the inner and outer shell boundaries and calculate the background corrected H alpha surface brightness of each object. We find significant differences in the shell shapes between the objects closest to the ionizing stars and those farther away. The closer group, which all represent proplyd interactions with the hypersonic stellar wind, have relatively closed shapes, while the farther group, which are due to interactions with the transonic ionized champagne flow in the nebula, are more open and hyperbolic. Although some of the latter group are also known proplyds, many are not, and the largest and brightest arcs tend to be associated with particularly luminous young stars, suggesting that the intrinsic T Tauri disk wind may play a role. The orientations of the arcs, together with the stagnation pressures estimated from the surface brightness, allow the internal velocity field of the H II region to be probed. We find that approximately radial flows from the core of the nebula dominate over disordered, turbulent flows.

1. INTRODUCTION

2. OBSERVATIONS

We have attempted to identify and characterize all stationary emission-line arcs in archival HST imaging observations of the Orion Nebula, obtained with the WFPC2 and ACS cameras, as summarized in Table 1. The primary dataset that we have used is the 26-orbit Cycle 12 program GO 9825 (Bally et al. 2006). This program covered a significant fraction of the entire nebula with the ACS/WFC camera in the filter F658N, which transmits the lines H α λ 6563 and [N II] λ 6584. The combination of good spatial resolution and signal-to-noise of this dataset makes it ideal for detecting the faint arcs against the varying nebular background. For regions in the outskirts of the nebula that are outside of the GO 9825 fields, we used observations with the same camera and filter from the 104-orbit Cycle 13 program GO 10246 (*HST* Treasury Program on the Orion Nebula Cluster, Robberto et al. 2013). In addition, we have used images from the same program obtained with the F656N filter of the WFPC2 camera. The resolution¹ and signal-to-noise of these observations is significantly worse than the ACS images, but they have the important advantage that the WFPC2 F656N filter is considerably narrower (≈ 5 Å) than the ACS F658N filter (≈ 15 Å) and suffers relatively little contamination from [N II]. Finally, for regions in the core of the nebula, we have used older WFPC2 images from programs GTO 5085 (O'Dell & Wong 1996) and GO 5469 (Bally et al. 1998). These offer two advantages for the study of the bowshocks closest to the Trapezium OB stars: shorter exposure times mean that the bright stars are less saturated, and images were obtained in a much wider range of emission line filters.

For each arc, we trace by eye the inner and outer boundaries of the emission line shell and mark along each edge using

¹ The point spread function is very similar for the two cameras (FWHM $\approx 0.082''$ at H α), but it is not well-sampled by the larger 0.1'' pixels of the three WFC chips of WFPC2.

“point” regions with the SAOimage ds9 program², and in addition mark the position of the central star or proplyd (hereafter, central source). These are shown in Figure 1 as yellow crosses, yellow pluses and blue circle for the outer edge, inner edge, and proplyd, respectively, for an illustrative case. We then fit circular arcs to the points, determining the center and radius of curvature R_c of each edge. The fits are carried out with the aid of the python library lmfit³, which implements a Levenberg–Marquardt curve-fitting algorithm. The initial parameter estimates for each fit are obtained as follows. First, the sky coordinates (α_i, δ_i) of the edge points are converted to polar coordinates with respect to the central source: (r_i, θ_i) , where θ is a position angle (degrees counterclockwise from north). After sorting the edge points in θ , the smallest value of r_i , together with its immediate neighbors to either side are used to define a parabola in polar coordinates, the root of whose derivative gives the point (r_0, θ_0) of closest approach of the arc’s edge to the central source.⁴ The initial estimate for the position of the center of curvature is taken to be the same distance from the central source as the point of closest approach, but on the “other side” of the source: that is at polar coordinates $(r_0, \theta_0 + 180^\circ)$. The sky coordinates of this center of curvature (α_c, δ_c) are the only two formal parameters of the circle fit since the circle radius is estimated on the fly as the mean distance $\langle R_c \rangle$ from (α_c, δ_c) to the individual edge points (α_i, δ_i) . Only those edge points satisfying the condition $|\theta_j - \theta_0| \leq 90^\circ$ are used in the fit.

3. CATALOG

3.1. LV knot group

² <http://ds9.si.edu>

³ <https://pypi.python.org/pypi/lmfit/>

⁴ This technique will fail if the closest edge point does not have a neighbor to one side, that is, if it is at one end of the traced edge. Such a situation is occasionally found when the observed arc is very asymmetric. In this case a parabola is fitted to all of the edge points (r_i, θ_i) in order to determine (r_0, θ_0) .

Table 1
Archival *HST* imaging datasets used in this study

Year	Instrument	Program(s)	Field size	Pixel size	Filters
1994–5	WFPC2/WFC	GTO 5085, GO 5469	5' × 10'	0.1"	F656N, F658N, F502N, F547M
1994–5	WFPC2/PC	GO 5469	1' × 2'	0.045"	F656N, F658N, F502N, F673N, F631N, F547M
2004	ACS/WFC	GO 9825	20' × 20'	0.05"	F658N
2004–5	ACS/WFC	GO 10246	25' × 30'	0.05"	F658N, F435W, F555W, F775W, F850LP
2004–5	WFPC2/WFC	GO 10246	25' × 30'	0.1"	F656N

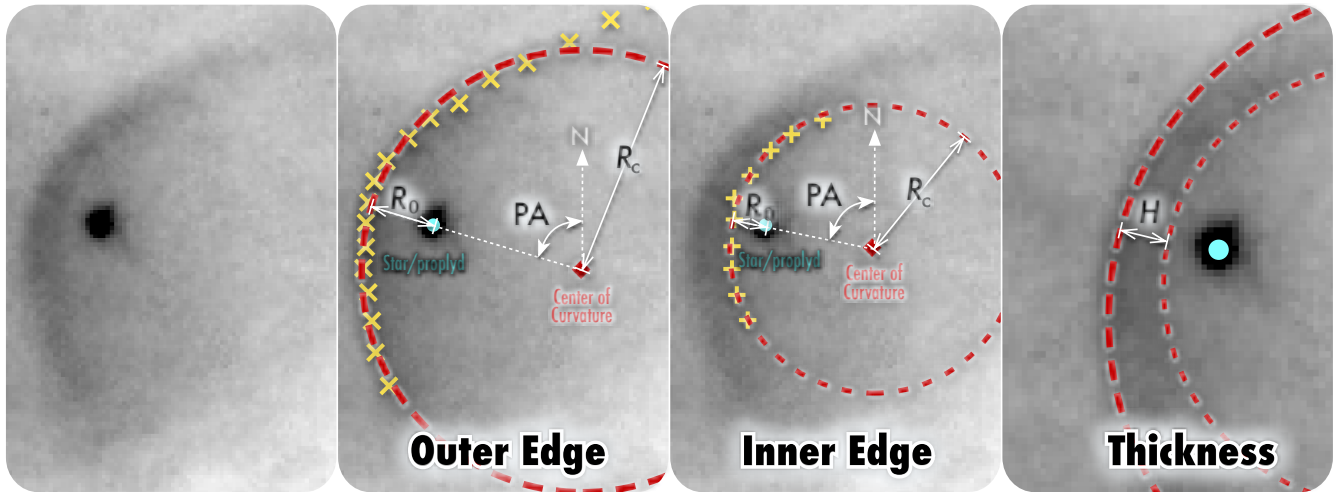


Figure 1. Methodology for determining geometric parameters of the arcs.

Table 2
Shell geometric parameters of lv knots

Object	RA	Dec	D	PA	R_{out}	R_{in}	$R_{\text{c,out}}$	$R_{\text{c,in}}$	h	PA_{out}	PA_{in}
158-323	05:35:15.83	-05:23:22.5	8.34	90.1	1.85	1.64	2.92	2.35	0.21	114.8	120.0
161-324	05:35:16.06	-05:23:24.3	5.29	70.1	1.16	0.90	3.01	2.03	0.26	70.7	76.6
163-317	05:35:16.28	-05:23:16.6	6.11	164.8	2.32	1.93	4.90	4.44	0.40	148.6	145.5
166-316	05:35:16.61	-05:23:16.2	7.15	207.0	0.69	0.41	1.19	0.85	0.28	181.4	160.5
167-317	05:35:16.74	-05:23:16.5	7.97	220.9	1.96	1.25	3.29	2.05	0.71	178.1	165.4
168-328	05:35:16.76	-05:23:28.1	7.79	315.2	1.06	0.79	1.31	0.80	0.27	345.3	353.0
168-326	05:35:16.84	-05:23:26.3	7.71	299.5	0.95	0.74	3.04	3.01	0.20	314.5	328.1

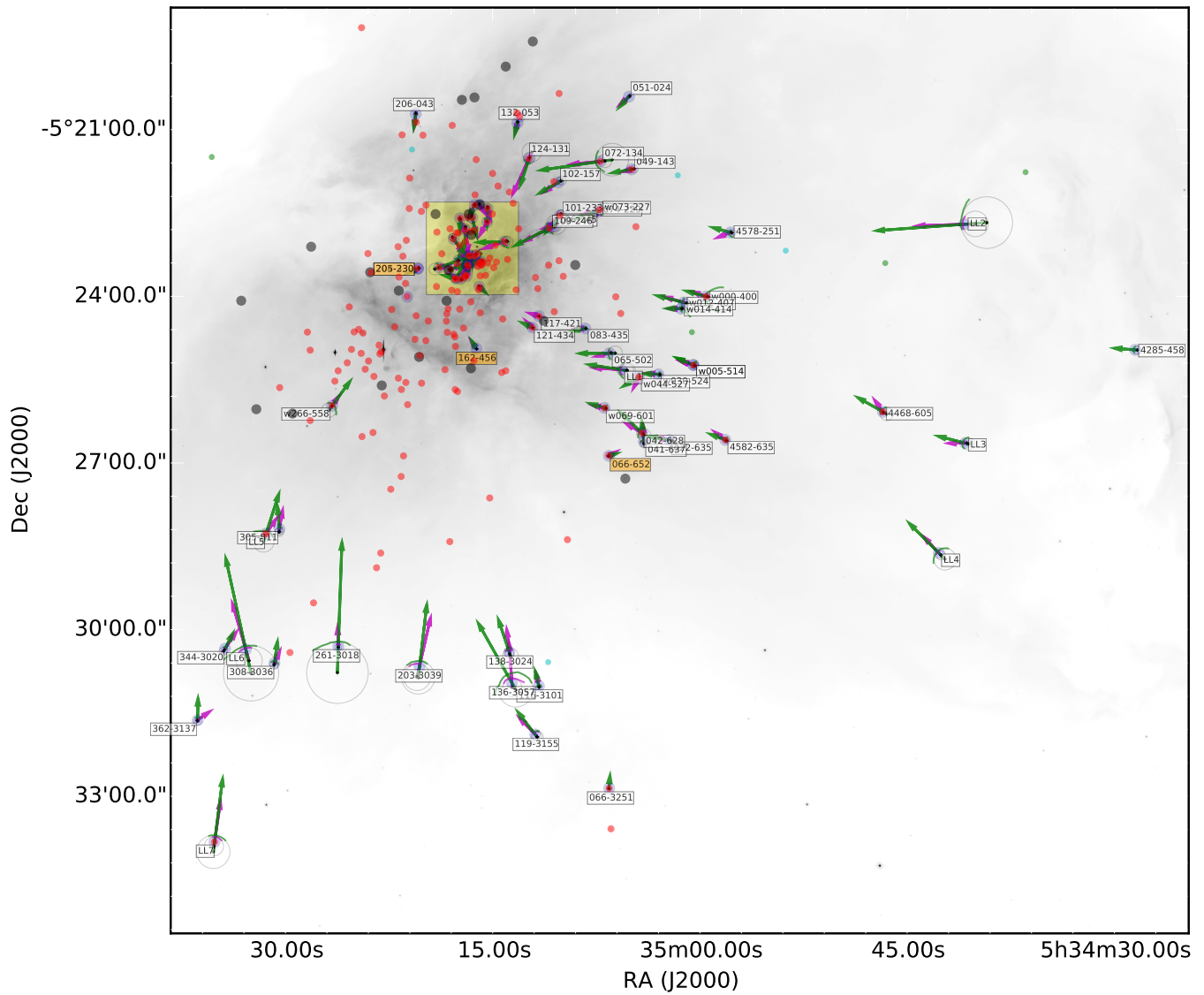


Figure 2. Position of bow shock arcs.

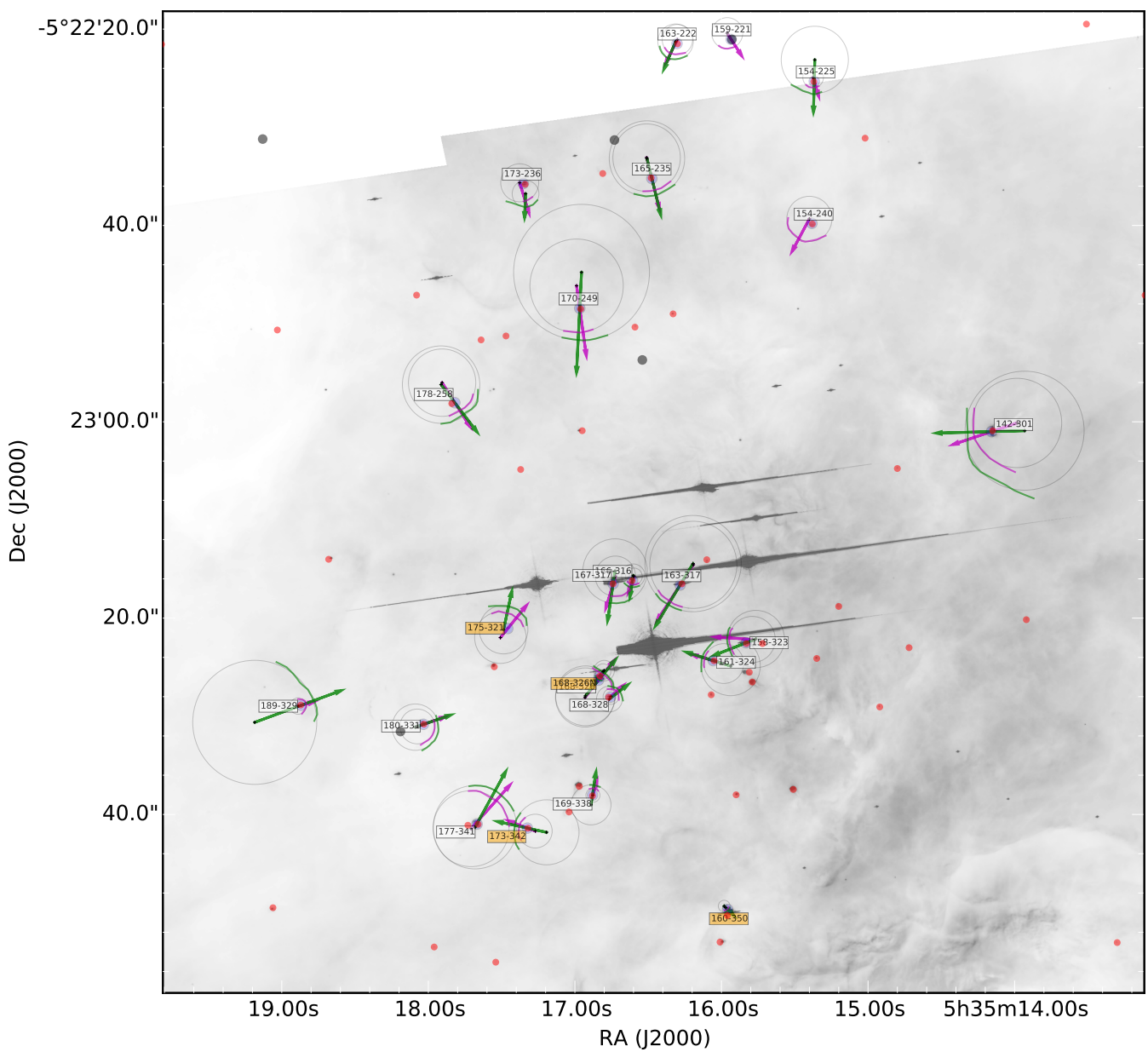


Figure 3. Position of bow shock arcs. Zoomed area.

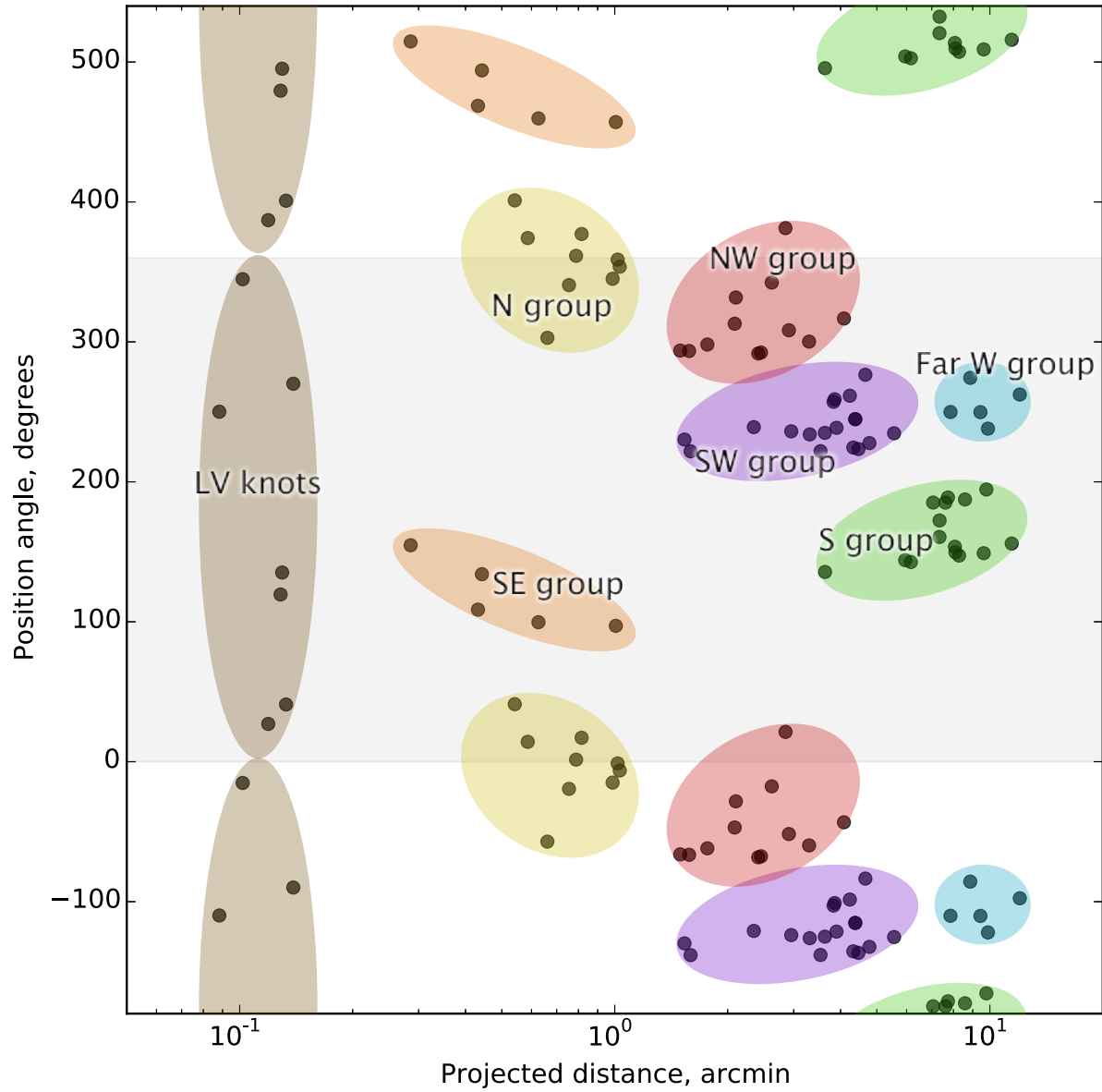


Figure 4. Spatial distribution of the bowshock arcs and classification into spatial groups.

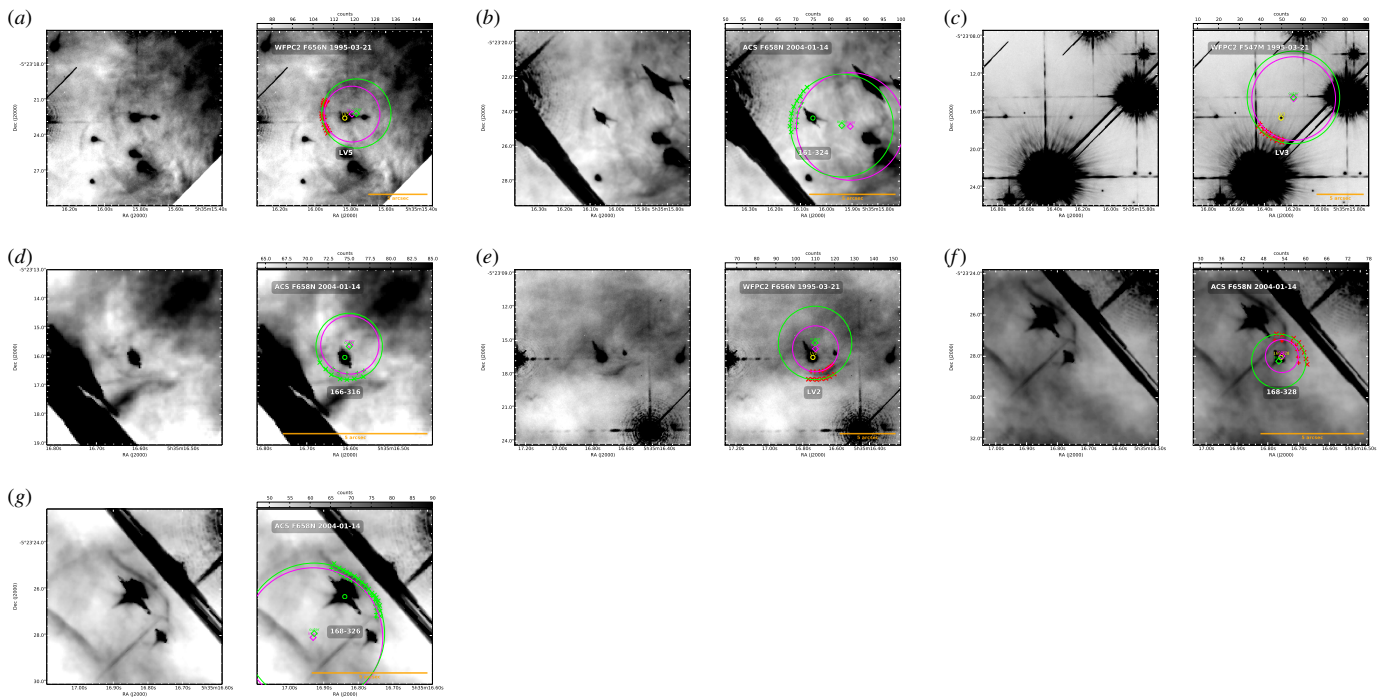


Figure 5. Stationary arc sources in the LV knots group.

3.2. *Southeast group*

Table 3
Shell geometric parameters of southeast group

Object	RA	Dec	D	PA	R_{out}	R_{in}	$R_{\text{c,out}}$	$R_{\text{c,in}}$	h	PA_{out}	PA_{in}
169-338	05:35:16.88	-05:23:38.0	17.14	334.7	1.03	0.68	2.04	0.72	0.35	345.9	6.4
177-341	05:35:17.67	-05:23:41.0	26.54	314.0	3.81	3.06	4.25	3.87	0.75	317.0	293.7
180-331	05:35:18.03	-05:23:30.8	25.91	288.7	1.44	1.11	2.36	1.77	0.33	280.8	282.0
189-329	05:35:18.87	-05:23:28.9	37.56	279.7	1.40	0.54	6.32	0.83	0.86	296.4	264.0

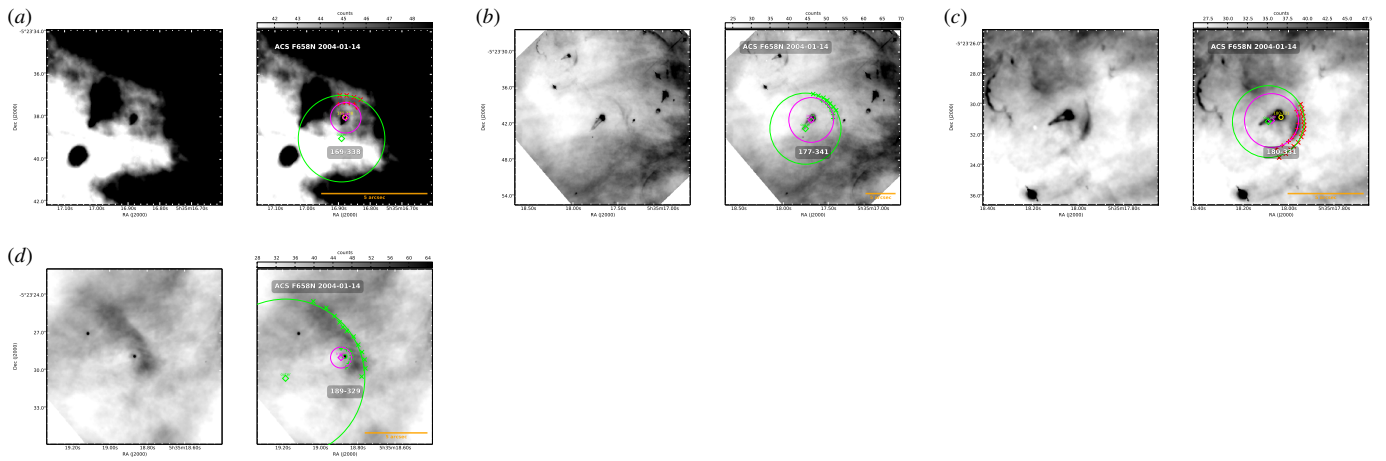


Figure 6. Stationary arc sources in the Southeast group.

3.3. *North group*

Table 4
Shell geometric parameters of north group

Object	RA	Dec	D	PA	R_{out}	R_{in}	$R_{\text{c,out}}$	$R_{\text{c,in}}$	h	PA_{out}	PA_{in}
142-301	05:35:14.16	-05:23:01.0	39.67	122.9	2.42	1.82	6.06	4.55	0.60	91.5	98.6
154-225	05:35:15.37	-05:22:25.3	59.22	165.1	1.29	0.64	3.42	1.05	0.58	158.0	193.1
154-240	05:35:15.38	-05:22:39.8	45.30	160.6	...	1.72	...	2.30	202.3
159-221	05:35:15.93	-05:22:21.0	61.86	173.7	...	0.83	...	1.58	215.4
163-222	05:35:16.30	-05:22:21.5	61.07	178.8	1.54	1.11	1.80	1.55	0.36	198.9	180.1
165-235	05:35:16.48	-05:22:35.2	47.33	181.5	1.78	1.23	3.84	3.44	0.47	197.5	193.2
170-249	05:35:16.97	-05:22:48.4	35.16	194.2	3.23	2.45	6.92	4.75	0.78	173.4	193.3
173-236	05:35:17.35	-05:22:35.7	48.96	197.1	2.28	1.53	1.36	1.94	0.75	255.3	275.5
178-258	05:35:17.82	-05:22:58.1	32.47	221.1	1.48	0.92	3.94	3.43	0.52	218.7	210.3

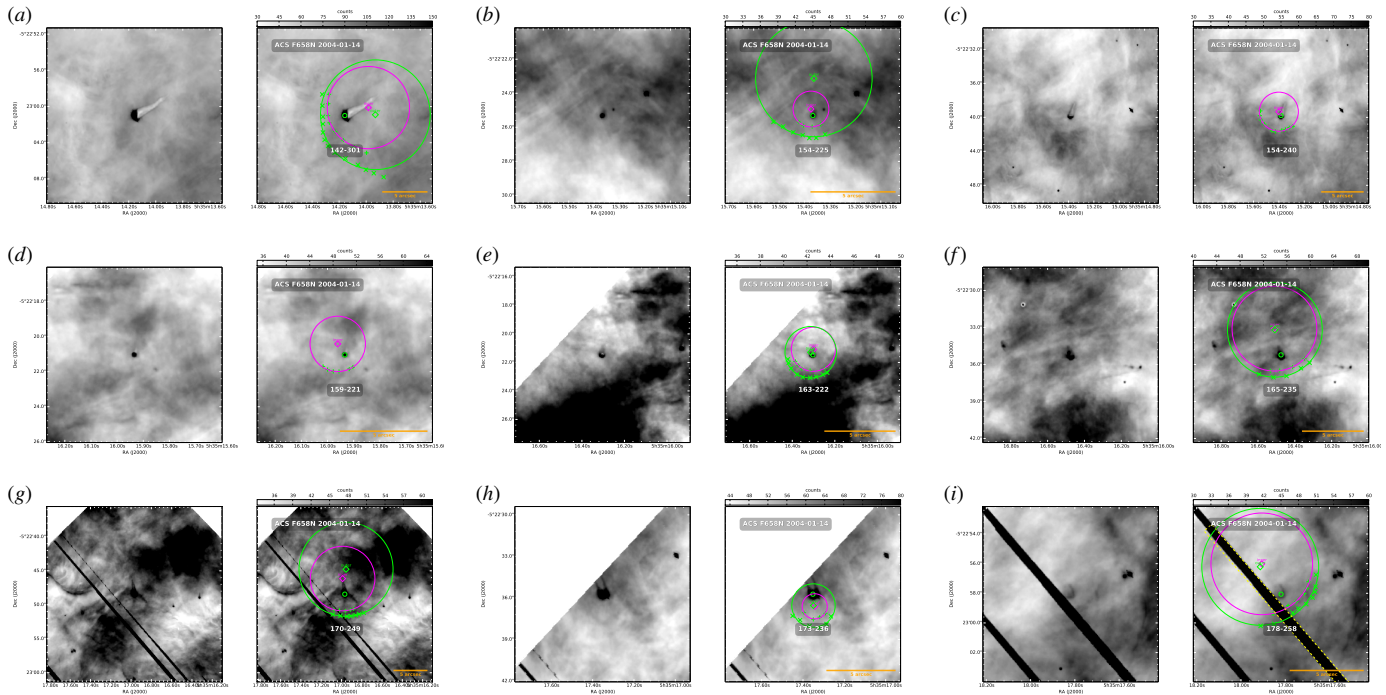


Figure 7. Stationary arc sources in the North group.

3.4. Northwest group

Table 5
Shell geometric parameters of northwest group

Object	RA	Dec	D	PA	R_{out}	R_{in}	$R_{c,\text{out}}$	$R_{c,\text{in}}$	h	PA_{out}	PA_{in}
4578-251	05:34:57.79	-05:22:51.1	279.49	96.5	1.85	1.19	3.52	2.07	0.53	81.2	125.0
049-143	05:35:04.94	-05:21:42.9	197.82	120.2	1.17	0.62	4.18	0.66	0.56	103.1	139.0
051-024	05:35:05.13	-05:20:24.3	245.01	136.7	1.19	0.90	2.29	1.66	0.27	136.5	123.6
072-134	05:35:07.20	-05:21:34.3	174.74	128.3	4.69	2.26	17.63	7.29	2.42	89.7	94.5
w073-227	05:35:07.27	-05:22:26.5	147.27	112.4	1.63	0.81	6.46	3.98	0.70	117.0	120.5
074-229	05:35:07.38	-05:22:28.9	144.78	111.7	1.36	0.79	1.60	0.75	0.60	120.3	185.7
101-233	05:35:10.13	-05:22:32.6	105.94	118.1	2.46	2.11	4.36	4.21	0.42	131.4	136.6
102-157	05:35:10.25	-05:21:57.1	125.30	133.0	0.80	0.40	5.03	3.54	0.45	118.5	116.6
106-245	05:35:10.58	-05:22:44.7	94.70	113.5	0.63	0.23	2.48	1.12	0.38	122.7	99.0
109-246	05:35:10.90	-05:22:46.3	89.68	113.8	1.95	1.32	10.64	7.33	0.70	112.9	119.5
124-131	05:35:12.38	-05:21:31.4	126.20	151.7	4.48	2.74	5.95	10.41	1.73	134.9	156.0
132-053	05:35:13.20	-05:20:52.6	157.31	162.4	0.72	0.32	1.80	0.68	0.39	153.9	167.0
206-043	05:35:20.56	-05:20:43.1	171.16	201.3	1.61	1.12	2.19	2.08	0.44	176.1	182.7

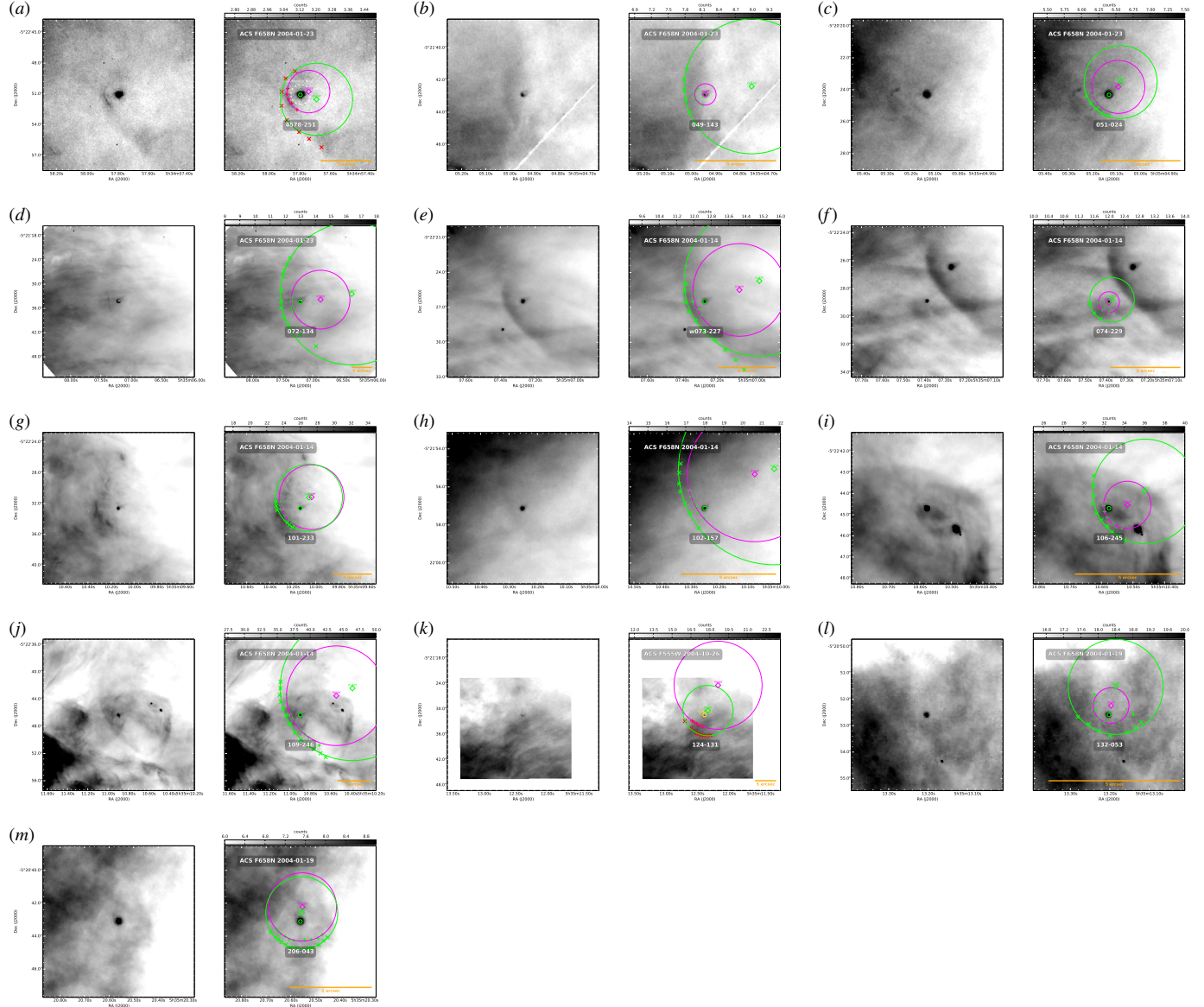


Figure 8. Stationary arc sources in the Northwest group.

3.5. Southwest group

Table 6
Shell geometric parameters of southwest group

Object	RA	Dec	D	PA	R_{out}	R_{in}	$R_{c,\text{out}}$	$R_{c,\text{in}}$	h	PA_{out}	PA_{in}
4582-635	05:34:58.17	-05:26:35.1	333.37	54.7	1.11	0.68	2.93	2.06	0.46	65.7	50.5
w000-400	05:34:59.57	-05:24:00.1	254.03	81.5	1.47	0.80	4.37	2.43	0.68	71.9	73.4
w005-514	05:35:00.47	-05:25:14.3	262.72	64.8	1.65	1.20	3.45	2.03	0.44	64.5	57.9
w005-514	05:35:00.47	-05:25:14.2	262.64	64.8	1.67	1.17	2.24	2.21	0.42	91.0	56.9
w012-407	05:35:01.17	-05:24:06.7	231.47	79.0	2.29	0.95	6.74	4.26	1.23	68.3	69.7
w014-414	05:35:01.37	-05:24:13.4	229.95	77.2	1.21	0.37	2.19	1.61	0.70	98.3	93.2
022-635	05:35:02.20	-05:26:35.3	286.47	47.7	1.10	0.75	4.46	2.29	0.34	83.2	77.5
w030-524	05:35:03.00	-05:25:24.4	234.09	58.6	0.63	0.29	2.56	1.54	0.32	93.8	82.0
041-637	05:35:04.06	-05:26:37.1	267.84	43.4	1.94	1.19	4.39	3.23	0.77	4.2	15.5
042-628	05:35:04.20	-05:26:27.6	259.59	44.5	3.07	1.76	6.90	3.61	1.34	61.6	56.1
w044-527	05:35:04.43	-05:25:27.4	217.94	55.0	2.13	0.78	3.25	1.53	0.85	121.2	267.4
LL1	05:35:05.64	-05:25:19.4	198.63	53.9	3.06	1.90	8.72	7.13	1.13	84.4	78.1
065-502	05:35:06.54	-05:25:01.5	177.29	56.1	1.42	0.49	7.74	2.31	1.21	90.5	104.7
w069-601	05:35:06.91	-05:26:00.6	212.19	41.9	0.85	0.41	2.72	1.77	0.42	86.1	87.1
083-435	05:35:08.29	-05:24:34.9	140.89	59.1	1.25	0.54	2.00	0.66	0.58	84.0	40.5
117-421	05:35:11.65	-05:24:21.4	92.07	50.2	...	0.71	...	0.93	96.7
121-434	05:35:12.12	-05:24:33.8	95.58	41.8	0.76	0.34	1.41	0.69	0.39	65.4	66.2

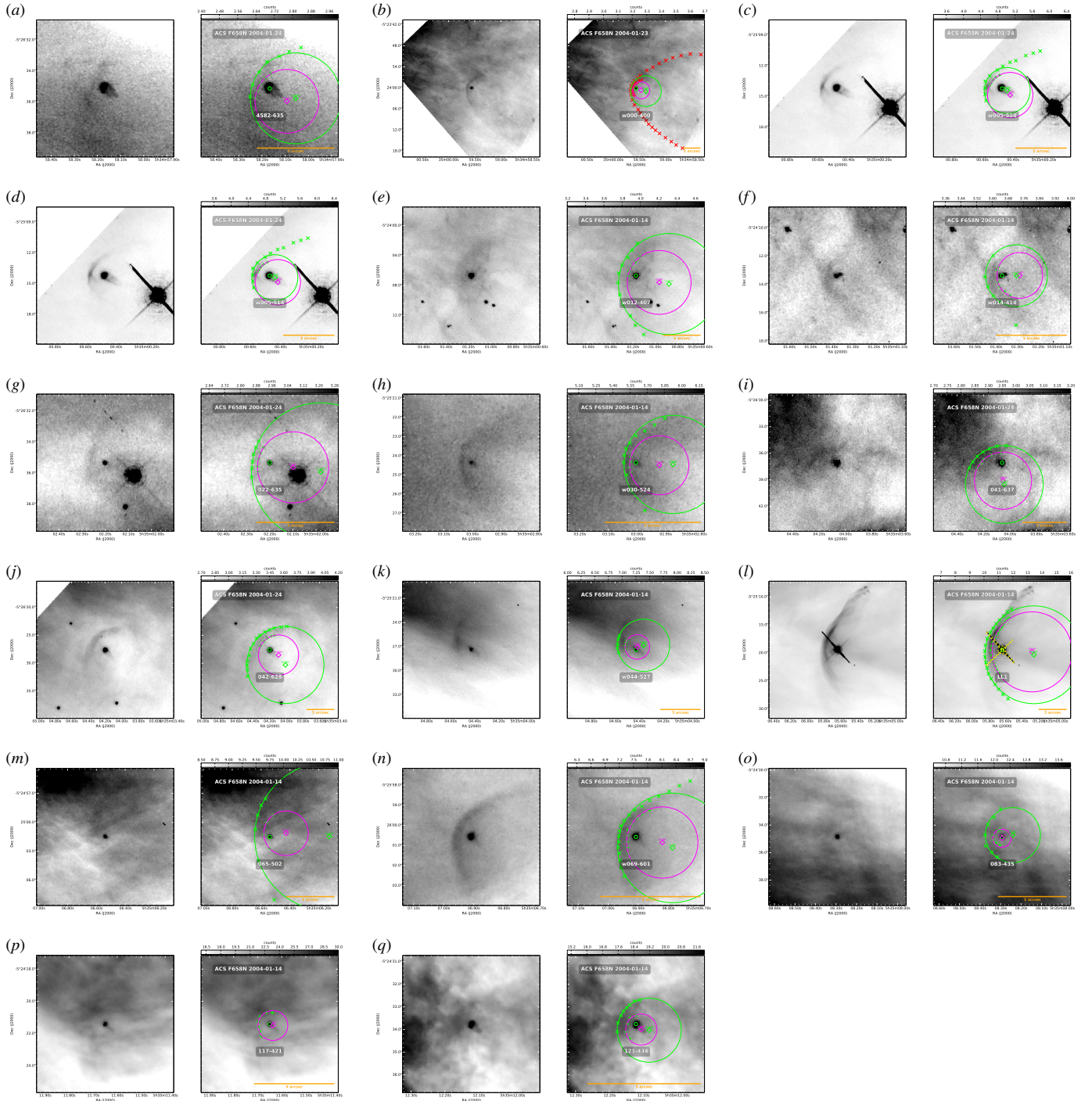


Figure 9. Stationary arc sources in the Southwest group.

3.6. *West group*

Table 7
Shell geometric parameters of west group

Object	RA	Dec	D	PA	R_{out}	R_{in}	$R_{c,\text{out}}$	$R_{c,\text{in}}$	h	PA_{out}	PA_{in}
4285-458	05:34:28.52	-05:24:57.9	721.18	82.4	1.91	...	4.34	87.0	...
LL3	05:34:40.81	-05:26:38.5	566.33	69.8	3.12	1.28	6.54	3.08	1.83	89.2	99.6
LL2	05:34:40.86	-05:22:42.2	532.12	94.3	4.04	2.07	27.93	13.84	1.13	97.6	89.5
LL4	05:34:42.72	-05:28:37.2	593.11	58.0	2.42	1.42	11.79	4.95	0.99	46.7	40.3
4468-605	05:34:46.76	-05:26:04.8	471.30	69.9	2.47	1.33	7.11	2.22	1.20	54.2	59.6

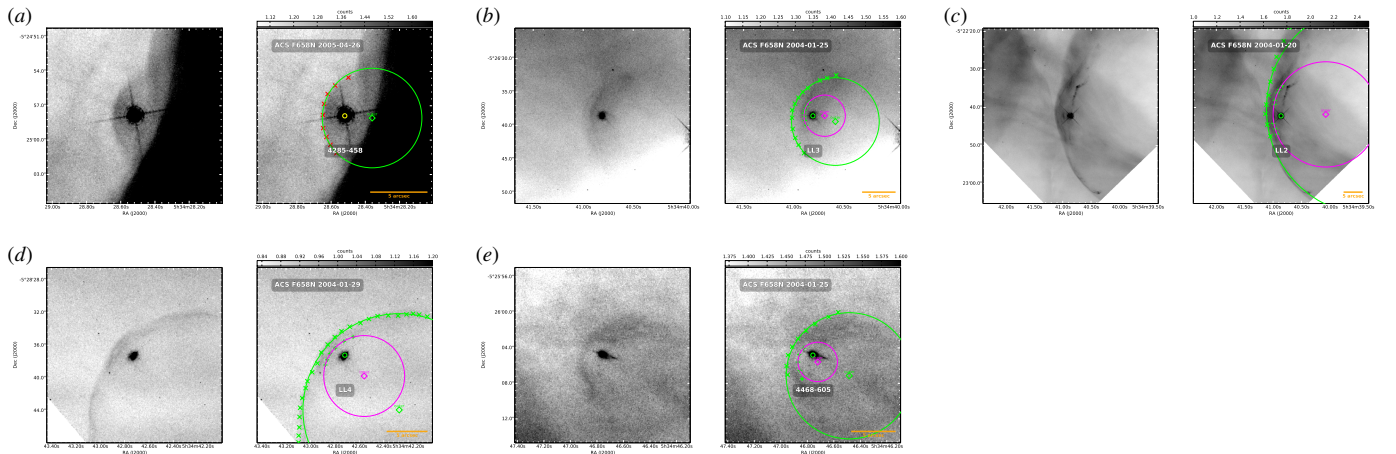


Figure 10. Stationary arc sources in the West group.

3.7. South group

Table 8
Shell geometric parameters of south group

Object	RA	Dec	D	PA	R_{out}	R_{in}	$R_{\text{c,out}}$	$R_{\text{c,in}}$	h	PA_{out}	PA_{in}
066-3251	05:35:06.57	-05:32:51.4	587.49	14.5	1.07	...	1.59	300.1	...
116-3101	05:35:11.65	-05:31:01.0	463.92	8.8	1.45	1.00	2.69	1.57	0.44	24.0	7.9
119-3155	05:35:11.93	-05:31:53.3	515.10	7.4	3.02	1.95	6.73	5.11	1.00	33.3	35.3
136-3057	05:35:13.61	-05:30:57.6	456.93	5.2	10.13	4.91	18.71	10.20	4.51	10.9	4.4
138-3024	05:35:13.80	-05:30:24.4	423.64	5.2	3.89	2.74	8.54	4.79	1.11	22.2	17.4
203-3039	05:35:20.29	-05:30:39.4	440.72	352.4	5.38	1.76	17.90	14.50	3.06	359.4	8.2
261-3018	05:35:26.17	-05:30:18.0	440.40	340.6	4.99	2.51	33.29	3.59	2.59	1.7	357.1
w266-558	05:35:26.62	-05:25:58.3	218.16	315.6	1.88	1.13	7.76	1.51	0.78	330.7	298.5
305-811	05:35:30.44	-05:28:11.2	356.86	324.0	1.72	0.89	4.92	3.99	0.80	358.6	349.7
308-3036	05:35:30.79	-05:30:36.3	484.13	333.6	2.56	1.44	4.50	1.78	1.12	359.9	329.8
LL5	05:35:31.40	-05:28:16.4	369.54	322.7	2.96	1.46	11.58	3.52	1.49	339.7	339.7
LL6	05:35:32.87	-05:30:21.5	485.82	329.6	3.63	1.63	29.90	14.20	2.05	7.6	18.0
344-3020	05:35:34.36	-05:30:20.6	496.76	327.3	1.66	0.67	3.15	4.42	0.95	334.9	325.5
LL7	05:35:35.13	-05:33:49.2	686.23	335.9	7.00	5.53	17.96	10.31	1.46	359.2	3.8
362-3137	05:35:36.35	-05:31:37.8	577.96	329.0	3.12	1.57	4.25	2.22	1.47	6.4	267.8

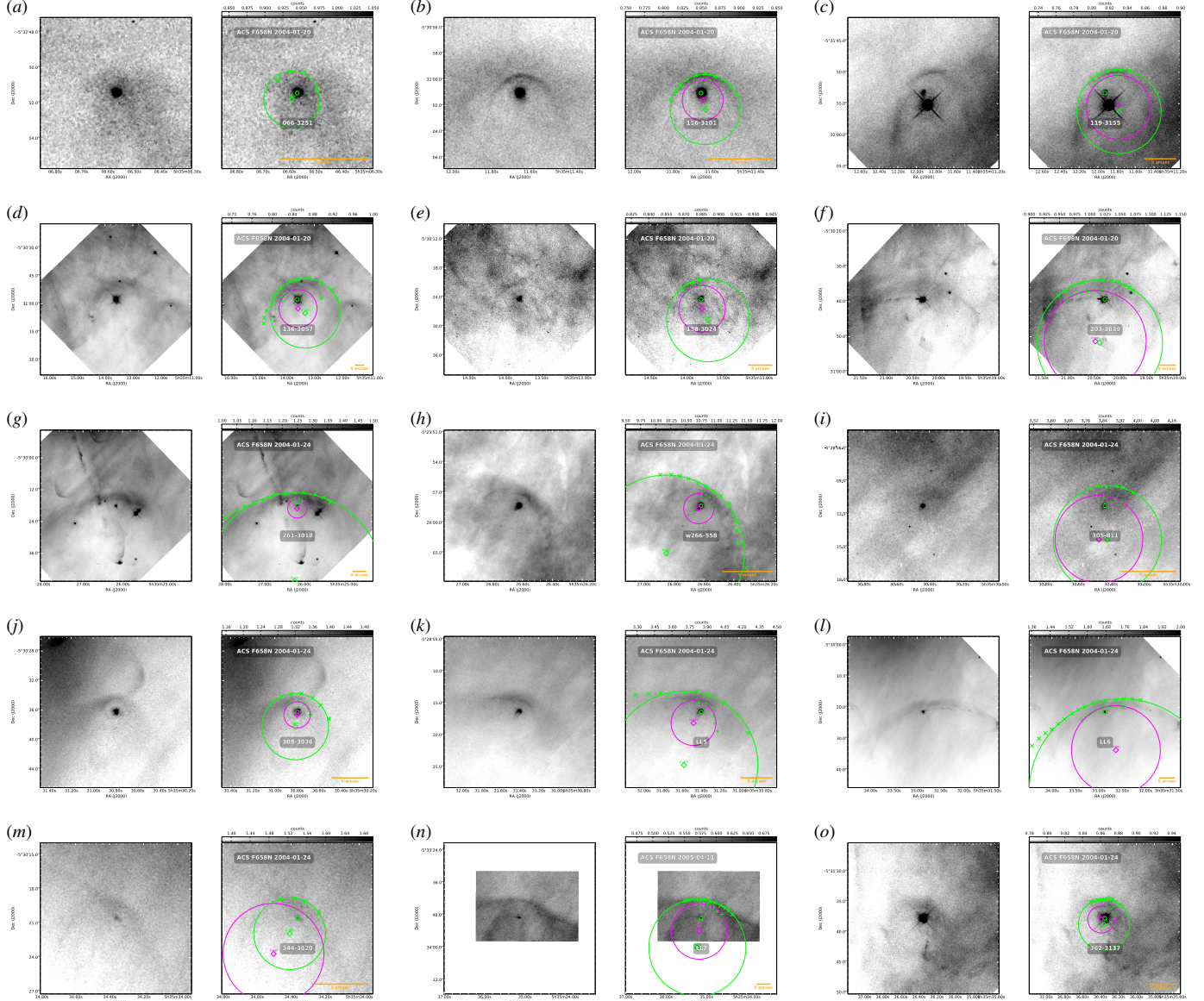


Figure 11. Stationary arc sources in the South group.

3.8. *Interproplyd shells*

Table 9
Shell geometric parameters of interproplyd shells

Object	RA	Dec	D	PA	R_{out}	R_{in}	$R_{\text{c,out}}$	$R_{\text{c,in}}$	h	PA_{out}	PA_{in}
066-652	05:35:06.59	-05:26:52.4	255.85	34.9	0.03	-0.07	0.57	0.60	0.10	316.8	341.9
160-350	05:35:15.96	-05:23:49.7	27.91	13.3	0.11	0.04	0.60	0.29	0.07	226.2	224.3
162-456	05:35:16.18	-05:24:56.4	93.91	1.9	0.29	0.21	0.85	0.79	0.09	28.8	49.2
168-326N	05:35:16.83	-05:23:26.0	7.49	297.4	0.23	0.12	1.04	0.79	0.11	137.0	142.2
173-342	05:35:17.32	-05:23:41.4	23.46	323.5	1.29	0.83	3.31	1.72	0.46	82.2	76.1
175-321	05:35:17.46	-05:23:21.1	16.03	264.7	2.03	1.38	2.48	2.63	0.60	298.7	324.5
204-330	05:35:20.40	-05:23:30.0	60.39	277.1	0.33	0.11	1.34	1.28	0.22	112.4	119.0

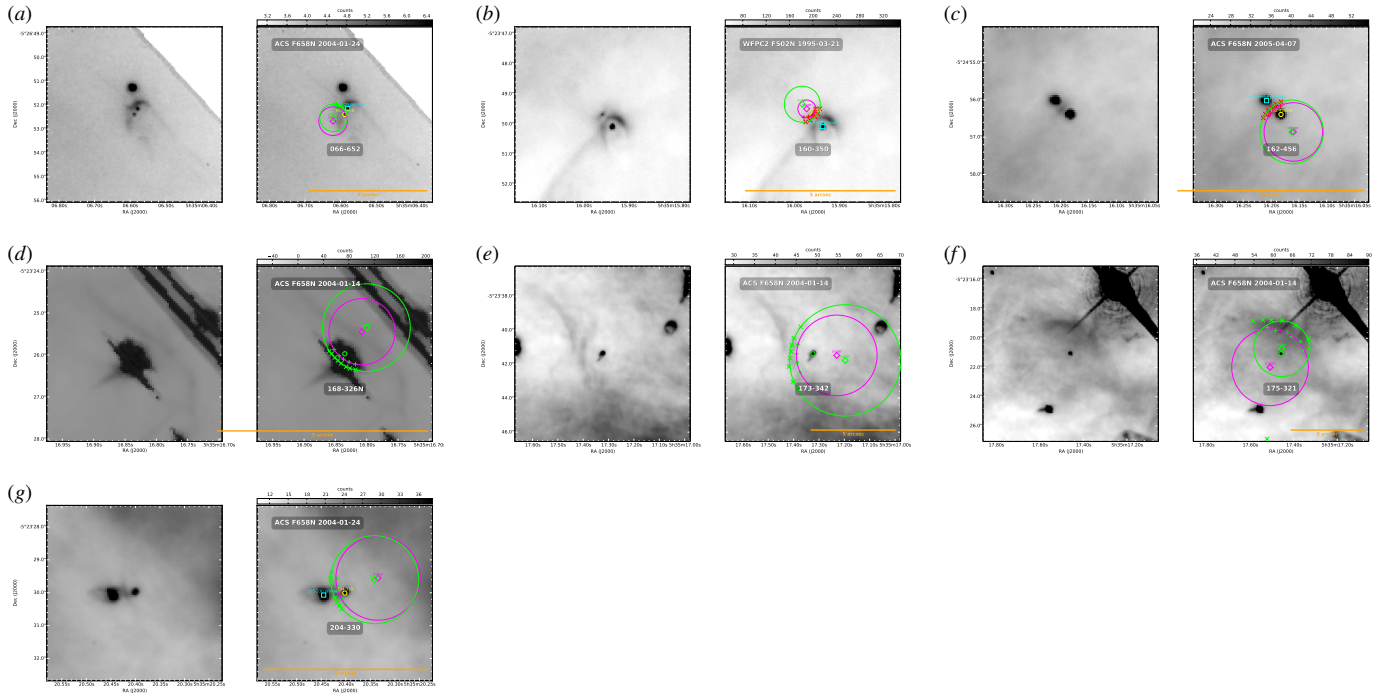


Figure 12. Stationary arc sources in the Interproplyd shells.

3.9. *probably not shells*

Table 10
Shell geometric parameters of problematic objects

Object	RA	Dec	D	PA	R_{out}	R_{in}	$R_{c,\text{out}}$	$R_{c,\text{in}}$	h	PA_{out}	PA_{in}
131-046	05:35:13.06	-05:20:45.8	164.46	162.4	3.55	1.00	7.33	5.64	2.17	140.3	144.2
212-400	05:35:21.18	-05:24:00.5	80.99	297.9	1.07	0.84	0.83	0.52	0.21	331.2	335.5

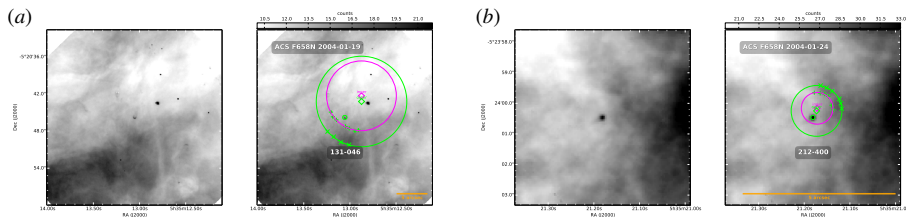


Figure 13. Stationary arc sources in the Problematic objects.

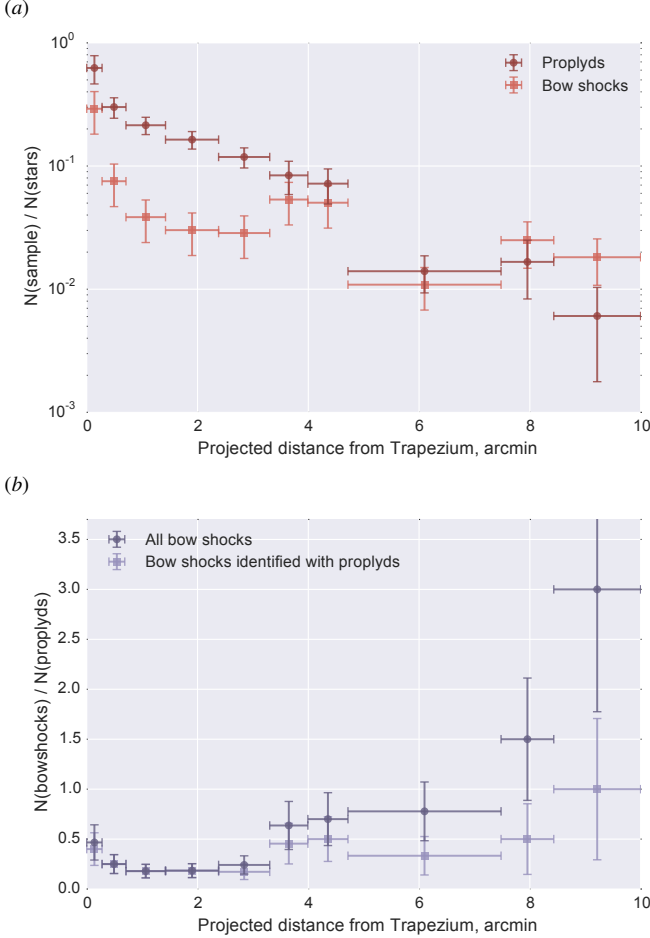


Figure 14. (a) Fraction of all optically visible stars that are proplyds (dark circle symbols) or have bowshocks (light square symbols) as a function of projected separation from the Trapezium. (b) Ratio between number of bowshocks and number of proplyds as a function of projected separation from the Trapezium. Dark circle symbols show all bowshocks in our catalog (with the exception of interproplyd shocks) while light square symbols show only those bowshocks associated with known or suspected proplyds.

4. DISCUSSION

Proplyd over star fraction falls off relatively smoothly with projected distance. Albeit with a sudden drop after about 200 arcsec.

Bowshock over proplyd fraction seems to have three separate peaks. Very small distances corresponding to the wind-wind interaction, then there is a dearth of bowshocks until a second peak around four arcmin. Finally at very large radii there may be a third peak of objects that are not proplyds.

But an alternate explanation for the third peak could be that they are all proplyds but that the proplyd fraction is underestimated at large distances.

On the other hand there is also evidence for three distinct populations from the azimuthal distribution around the Trapezium. The group at 4 arcmin separation are mainly to the west whereas the more distant objects are mainly to the south.

REFERENCES

- Bally, J., Licht, D., Smith, N., & Walawender, J. 2006, AJ, 131, 473
- Bally, J., Sutherland, R. S., Devine, D., & Johnstone, D. 1998, AJ, 116, 293
- O'Dell, C. R., & Wong, K. 1996, AJ, 111, 846
- Robberto, M., et al. 2013, ApJS, 207, 10

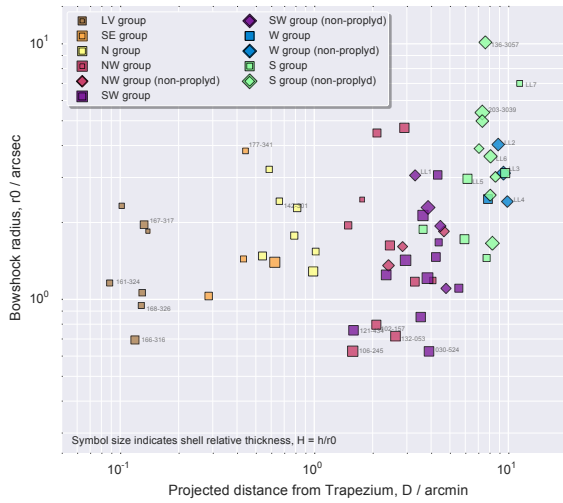


Figure 15. Bowshock axial size versus distance from the Trapezium.

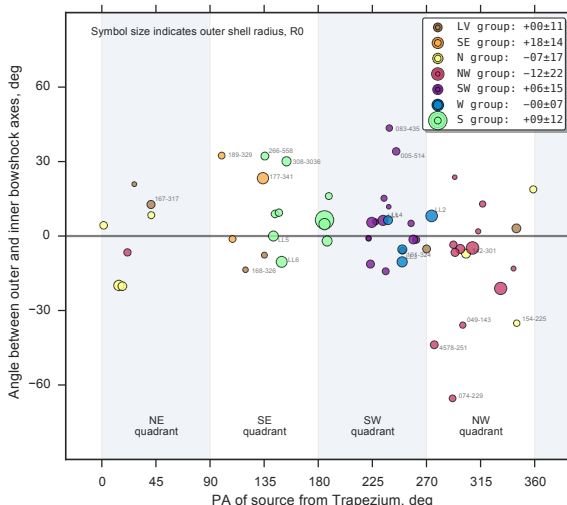
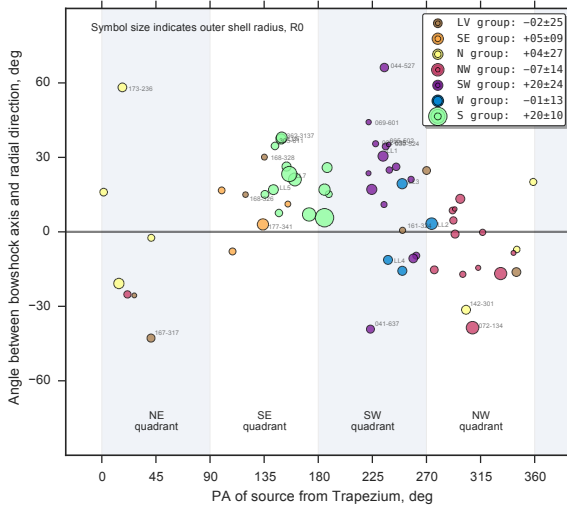


Figure 16. Angle offset between bowshock axis and the radial direction to θ^1 Ori C .

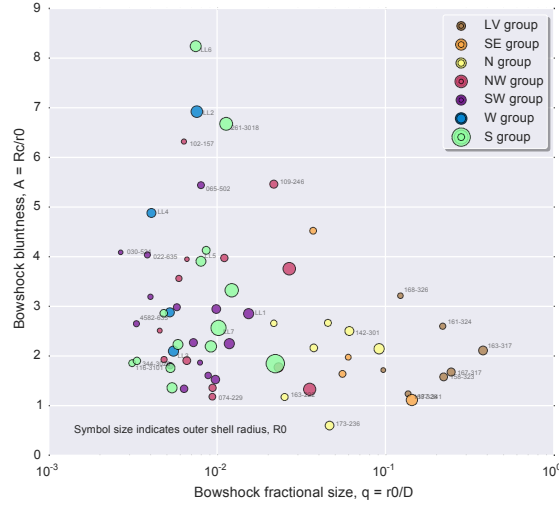


Figure 17. Bowshock bluntness versus relative size.

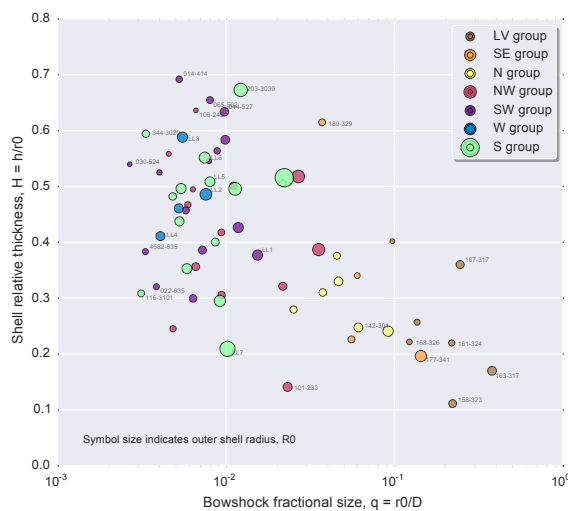


Figure 18. Bowshock relative shell thickness versus relative size.